
# Chapter 28
# Cavity Flow of a Micropolar Fluid - a Parameter Study

Wilhelm Rickert & Sebastian Glane

**Abstract** This paper presents a parameter study of the flow of a micropolar fluid. The underlying equations and the choice of boundary conditions are discussed. Two flow situations are considered: Couette flow as a reference problem and the lid-driven cavity problem. The governing equations are specialized for the case of two-dimensional flow and discussed in dimensionless form. Several dimensionless parameters common in the theory of micropolar fluids are identified and their impact on the solutions is analyzed using the finite element method.

**Keywords:** Micropolar fluid theory · Microstructured material · Lid-driven cavity problem · Forced convection

## 28.1 Introduction

Generalized continuum theories have gained high interest in continuum mechanics and material modeling. Among Cosserat elasticity and gradient theories for solids and the Ericksen-Leslie theory for liquid crystals, Eringen's micropolar theory is one of the representatives of this field, see Ariman et al (1973) for an extensive review and Maugin (2011) for a historical discussion. Since its introduction by Eringen (1964), the theory of micropolar fluids has been widely applied, for example in the modeling of blood, Ariman et al (1973), particle suspensions, liquid crystals, lubrication, Prakash and Sinha (1975), and colloidal suspensions, Eringen (1991). In a series of papers, Müller and Vilchevskaya extended micropolar theory and investigated the production of microinertia, see Müller and Vilchevskaya (2017); Müller et al (2017); Müller and Vilchevskaya (2018); Vilchevskaya and Müller (2018). This extension may be applied to problems with microstructural changes.

Wilhelm Rickert · Sebastian Glane
Technische Universität Berlin, Institute of Mechanics, Einsteinufer 5, 10587 Berlin, Germany,
e-mail: rickert@tu-berlin.de, glane@tu-berlin.de



B. E. Abali et al. (eds.), *New Achievements in Continuum Mechanics and Thermodynamics*, Advanced Structured Materials 108,
https://doi.org/10.1007/978-3-030-13307-8_28

In this study the effect of micropolar material parameters is investigated through parameter variations using a numerical model. The flow problem considered in the parameter study is the lid-driven cavity problem. This is a (benchmark) problem in fluid mechanics. Many authors report numerical solutions for the flow of a Navier–Stokes fluid in a two or three dimensional cavity using different numerical techniques, see Botella and Peyret (1998); Bruneau and Saad (2006); Cortes and Miller (1994); Erturk and Gökccöl (2008); Freitas et al (1985); Nallasamy and Prasad (1977). Furthermore, this problem was studied for a thermally-driven flow of a buoyant fluid using the Boussinesq approximation, Iwatsu and Hyun (1995); Kareem et al (2016); Le Quere et al (1981), for nanofluids, Tiwari and Das (2007), and also for multiphase flow, Anders and Weinberg (2011); Chakravarthy and Ottino (1996). In context of micropolar fluids, thermally-driven convection was studied for cavities with different geometrical shapes, Aydin and Pop (2007); Bourantas and Loukopoulos (2014); Gibanov et al (2016a,b); Hsu and Chen (1996); Jena and Bhatacharyya (1986); Sheremet et al (2017), and including electromagnetic fields, Türk and Tezer-Sezgin (2017). Most of the papers on the micropolar cavity problem are concerned with the influence of micropolar parameters on the onset of convection (critical Rayleigh number), on the heat transfer and effects of the "vortex viscosity" on the heat generation. However, a parameter study neglecting thermal effects and only focusing on the mechanical behavior has not yet been conducted to the best of the authors' knowledge.

Following a presentation of the theory of micropolar fluids in Sect. 28.2, two flow situations are considered: Couette flow as a reference problem and the lid-driven cavity flow. The governing equations are specialized for these two-dimensional problems in Sect. 28.3 and subsequently solved numerically using the finite element method. The numerical procedure is described in Sect. 28.4 and a convergence analysis is performed based on the analytical solution for the Couette flow. The parameter study is presented and discussed in Sect. 28.5 before a conclusion is given in Sect. 28.6.

## 28.2 Theory of Micropolar Fluids

In context of a generalized continuum theory, the balance equations of mass, momentum and energy are supplemented by additional balances for the fields of angular velocity and moment of inertia. This introduces additional flux terms as well as production terms in the balance equations and the constitutive equations are modified in order to account for effects associated to the additional fields. Moreover, additional constitutive equations for the coupled stress and the production terms are required. In this paper, the theory of micropolar fluids is employed, in which an additional independent rotational degree of freedom, namely the angular velocity field[1], $\boldsymbol{\omega}(\boldsymbol{x}, t)$, is introduced. In this framework, the microinertia tensor, $\boldsymbol{J}(\boldsymbol{x}, t)$, is

[1] The angular velocity field is sometimes also referred to as the microgyration vector, *cf.* Eringen (2001).

an additional field accounting for the inertia of the material against microrotation. Below, we present the equations governing micropolar fluids and neglect microinertia effects later on.

### 28.2.1 Governing Local Balance Equations

In spatial description, the governing local equations are the balances of mass, linear momentum, moment of inertia and spin (Müller and Vilchevskaya, 2018)

$$\frac{\mathrm{d}\rho}{\mathrm{d}t} = -\rho(\nabla \cdot \boldsymbol{v}) \,, \quad \rho\frac{\mathrm{d}\boldsymbol{v}}{\mathrm{d}t} = \nabla \cdot \boldsymbol{\sigma} + \rho\boldsymbol{f} \,, \quad \frac{\mathrm{d}\boldsymbol{J}}{\mathrm{d}t} = \boldsymbol{\omega} \times \boldsymbol{J} - \boldsymbol{J} \times \boldsymbol{\omega} + \boldsymbol{\chi} \,,$$
$$\rho\frac{\mathrm{d}}{\mathrm{d}t}\big(\boldsymbol{J} \cdot \boldsymbol{\omega}\big) = \nabla \cdot \boldsymbol{\mu} + \boldsymbol{\sigma} \cdot\!\cdot \overset{(3)}{\boldsymbol{\epsilon}} + \rho\boldsymbol{m} + \rho\boldsymbol{\chi} \cdot \boldsymbol{\omega} \,, \tag{28.1}$$

where $\rho$ is the density, $\boldsymbol{v}$ the velocity, $\boldsymbol{\sigma}$ the Cauchy stress tensor, $\boldsymbol{f}$ the specific body force, $\boldsymbol{J}$ the inertia tensor, $\boldsymbol{\mu}$ the couple stress tensor, $\boldsymbol{m}$ the specific volume couple, $\boldsymbol{\chi}$ the symmetric production of moment of inertia, and $\overset{(3)}{\boldsymbol{\epsilon}}$ the complete anti-symmetric tensor (density) of rank three. The standard scalar product of two tensors of second rank can be evaluated via $\boldsymbol{A} \cdot\!\cdot\, \boldsymbol{B} = A_{ij}B_{ij}$, where Einstein's summation convention applies and an orthonormal coordinate system is used. Furthermore, cross products of a second-rank tensor $\boldsymbol{A}$ and a vector $\boldsymbol{b}$ are given by $\boldsymbol{A} \times \boldsymbol{b} = (\boldsymbol{A} \otimes \boldsymbol{b}) \cdot\!\cdot\, \overset{(3)}{\boldsymbol{\epsilon}}$ and $\boldsymbol{b} \times \boldsymbol{A} = \overset{(3)}{\boldsymbol{\epsilon}} \cdot\!\cdot\, (\boldsymbol{b} \otimes \boldsymbol{A})$.[2]

This set of equations accounts for microstructural changes, because a production term, $\boldsymbol{\chi}$, is present in balance of the moment of inertia tensor. While such a production is not present in early works on micropolar fluids, see Eringen (1964, 1966), it was later introduced by Eringen (1985) to model a sticking of fluid to suspended rigid particles, see Eringen (1991, 1985); Zhilin (2006). Other examples for microstructural changes such as the crushing of particles, Glane et al (2017); Vilchevskaya and Müller (2018), the expansion of pressurized spherical particles, Müller and Vilchevskaya (2018), or the orientation and elongation of charged particles in an electric field, Müller and Vilchevskaya (2018), were proposed in a series of papers. Therein, different types of constitutive equations for the production term were studied. According to Zhilin (2006), the production term can be neglected, if the particles are considered rigid on the microscale. In summary, the question of whether or not the production term shall be included is a question of modeling of a specific fluid.

[2] In an orthonormal coordinate system, the components of this product may also be expressed as:

$$(\boldsymbol{A} \times \boldsymbol{b})_{ij} = A_{ik}b_l\varepsilon_{klj} \,.$$

### *28.2.2 Constitutive Laws and Field Equations*

The local balances stated in Eq. (28.1) need to be supplemented by suitable constitutive equations. In this study, the quantities $\boldsymbol{\chi}$, $\boldsymbol{g}$, and $\boldsymbol{m}$ are neglected later and linear constitutive relations for the flux terms $\boldsymbol{\sigma}$ and $\boldsymbol{\mu}$ are employed. For isotropic micropolar fluids the following constitutive relations were derived in, *e.g.*, Cowin (1974); Eringen (2001); Zhilin (2006) and are applied subsequently:

- The Cauchy stress tensor is given by

$$\boldsymbol{\sigma} = (-p + \lambda \nabla \cdot \boldsymbol{v})\mathbf{1} + 2\mu \boldsymbol{D} - 2\tau(\boldsymbol{W} + \overset{(3)}{\boldsymbol{\epsilon}} \cdot \boldsymbol{\omega}) \,, \tag{28.2}$$

  where $\boldsymbol{D}$ is the symmetric and $\boldsymbol{W}$ is the skew-symmetric part of the velocity gradient $\boldsymbol{v} \otimes \nabla$. In Eq. (28.2), $p$ denotes the thermodynamic pressure, $\lambda$ and $\mu$ the volume and shear viscosity, respectively, and $\tau$ is an additional viscosity associated to rotational shear, which also has the unit $\mathrm{kg\,m^{-1}\,s^{-1}}$. The vorticity, $\boldsymbol{w} = \nabla \times \boldsymbol{v}/2$, may be referred to as regional angular velocity, Cowin (1974), and is the axial vector of the skew-symmetric part of the velocity gradient with $\boldsymbol{W} = -\overset{(3)}{\boldsymbol{\epsilon}} \cdot \boldsymbol{w}$. Thus, the last term in Eq. (28.2) is a difference between the local angular velocity and the vorticity. Therefore, we may refer to $\tau$ as rotational shear viscosity. Note that, in the limiting case $\tau \to 0$, the constitutive relation of an ordinary Navier–Stokes fluid is recovered.
- The couple stress tensor can be written as:

$$\boldsymbol{\mu} = \alpha(\nabla \cdot \boldsymbol{\omega})\mathbf{1} + 2\beta \boldsymbol{Q} - 2\gamma \boldsymbol{R} \,, \tag{28.3}$$

  where $\boldsymbol{Q}$ is the symmetric and $\boldsymbol{R}$ the skew-symmetric part of the angular velocity gradient $\boldsymbol{\omega} \otimes \nabla$. Here, $\alpha$, $\beta$ and $\gamma$ are generalized viscosities that have the unit $\mathrm{kg\,m\,s^{-1}}$. The constitutive relations for the Cauchy stress and couple stress tensor is similar. However, it should be noted that the couple stress tensor, $\boldsymbol{\mu}$, does not have a direct functional dependency on the velocity field, which is not the case for the Cauchy stress tensor, $\boldsymbol{\sigma}$.

In the following, we restrict the analysis to constant material coefficients. Insertion of the constitutive equations specified above gives rise to the following field equations:

$$\begin{aligned}
0 = \frac{\mathrm{d}\rho}{\mathrm{d}t} + \rho(\nabla \cdot \boldsymbol{v}) \,, \quad \frac{\mathrm{d}\boldsymbol{J}}{\mathrm{d}t} &= \boldsymbol{\omega} \times \boldsymbol{J} - \boldsymbol{J} \times \boldsymbol{\omega} + \boldsymbol{\chi} \,, \\
\rho \frac{\mathrm{d}\boldsymbol{v}}{\mathrm{d}t} &= -\nabla p + (\lambda + \mu - \tau)\nabla[\nabla \cdot \boldsymbol{v}] + (\mu + \tau)\Delta \boldsymbol{v} + 2\tau \nabla \times \boldsymbol{\omega} + \rho \boldsymbol{f} \,, \\
\rho \frac{\mathrm{d}}{\mathrm{d}t}(\boldsymbol{J} \cdot \boldsymbol{\omega}) &= (\alpha + \beta - \gamma)\nabla[\nabla \cdot \boldsymbol{\omega}] + (\beta + \gamma)\Delta \boldsymbol{\omega} - 4\tau \boldsymbol{\omega} + \\
&\qquad + 2\tau \nabla \times \boldsymbol{v} + \rho \boldsymbol{m} + \rho \boldsymbol{\chi} \cdot \boldsymbol{\omega} \,,
\end{aligned} \tag{28.4}$$

where $\Delta$ is the Laplace operator.

According to Müller and Vilchevskaya (2018), the production of moment of inertia, $\boldsymbol{\chi}$, must be interpreted as an additional constitutive quantity. However, we restrict our investigations to rigid spherical particles (on the mesoscale). As a consequence, the moment of inertia tensor is a constant spherical tensor, *i.e.*, $\boldsymbol{J} = J_0\mathbf{1}$, the production of moment of inertia vanishes and Eq. $(28.4)_2$ is fulfilled trivially because $\boldsymbol{\omega} \times \boldsymbol{J} - \boldsymbol{J} \times \boldsymbol{\omega}$ vanishes. Additionally we assume that the micropolar fluid is incompressible, *i.e.*, the mass density is a constant, $\rho_0$. Moreover, we assume that the specific body force, $\boldsymbol{f}$, and the specific volume couple, $\boldsymbol{m}$, are negligible. Under these assumptions, Eqs. (28.4) reduce to:

$$\begin{aligned} \nabla \cdot \boldsymbol{v} = 0 \,, \quad \rho_0 \frac{\mathrm{d}\boldsymbol{v}}{\mathrm{d}t} &= -\nabla p + (\mu + \tau)\Delta \boldsymbol{v} + 2\tau \nabla \times \boldsymbol{\omega} \,, \\ \rho_0 J_0 \frac{\mathrm{d}\boldsymbol{\omega}}{\mathrm{d}t} &= (\alpha + \beta - \gamma)\nabla[\nabla \cdot \boldsymbol{\omega}] + (\beta + \gamma)\Delta \boldsymbol{\omega} + 2\tau \nabla \times \boldsymbol{v} - 4\tau \boldsymbol{\omega} \,. \end{aligned} \tag{28.5}$$

## 28.3 Problem Statement

In the following, two different problems of a stationary and two-dimensional flow of a micropolar fluid are considered. Figure 28.1 shows the two different problems. First, the Couette flow is considered as a reference problem, see Fig. 28.1a. For this problem, an analytical closed-form solution can be obtained for micropolar fluids, *cf.* Cowin (1974), which is subsequently used for a verification of the finite element method.

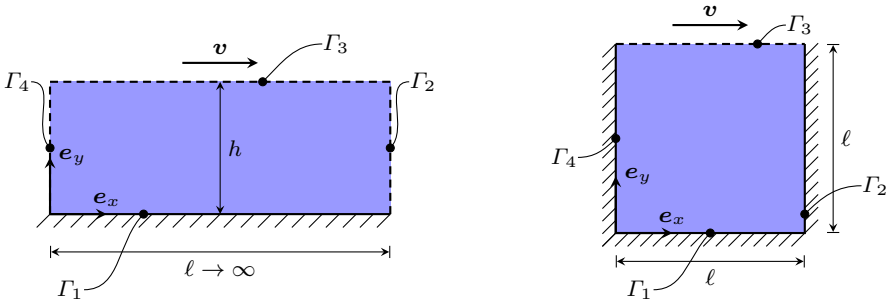


**(a)** Couette flow problem. **(b)** Lid-driven cavity problem.

**Fig. 28.1** Example problems.

The second problem is the lid-driven cavity problem, see Fig. 28.1b. At the top of the cavity, a "conveyor" modeled through purely tangential velocity forces a fluid motion in the underlying domain.

### *28.3.1 Dimensionless Equations*

The parameters present in the equations for micropolar fluids are the generalized viscosities $\alpha$, $\mu$, $\tau$, $\alpha$, $\beta$, $\gamma$ and the generalized inertias $\rho_0$, $J_0$. In order to determine the governing combinations of these material parameters, the problem is written in dimensionless form. The normalized quantities are introduced as:

$$\boldsymbol{x} = \ell_{\mathrm{ref}}\tilde{\boldsymbol{x}}\ , \quad \boldsymbol{v} = v_{\mathrm{ref}}\tilde{\boldsymbol{v}}\ , \quad t = t_{\mathrm{ref}}\tilde{t}\ , \quad p = p_{\mathrm{ref}}\tilde{p}\ , \quad \boldsymbol{\omega} = \omega_{\mathrm{ref}}\tilde{\boldsymbol{\omega}}\ , \tag{28.6}$$

where symbols with a tilde are dimensionless. As usual in fluid mechanics, the time scale is chosen as the time scale of convective transport, *i.e.*, $t_{\mathrm{ref}} = {}^{\ell_{\mathrm{ref}}}\!/_{v_{\mathrm{ref}}}$, and the pressure is normalized by $p_{\mathrm{ref}} = \rho_0 v_{\mathrm{ref}}^2$. Because of the fact that we will impose zero spin boundary conditions at walls, the angular velocity field, $\boldsymbol{\omega}$, is solely triggered by the velocity. It seems therefore reasonable to choose the reference angular velocity accordingly. Here, $\omega_{\mathrm{ref}} = {}^{v_{\mathrm{ref}}}\!/_{\ell_{\mathrm{ref}}}$ is applied to emphasize the influence of the velocity. As a consequence, the following dimensionless system of equations arises:

$$\begin{aligned} &\tilde{\nabla}\cdot\tilde{\boldsymbol{v}} = 0\ , \quad \frac{\mathrm{d}\tilde{\boldsymbol{v}}}{\mathrm{d}\tilde{t}} = -\tilde{\nabla}\tilde{p} + \frac{1}{(1-N^2)Re}\big(\tilde{\Delta}\tilde{\boldsymbol{v}} + 2N^2\tilde{\nabla}\times\tilde{\boldsymbol{\omega}}\big)\ , \\ &\frac{\mathrm{d}\tilde{\boldsymbol{\omega}}}{\mathrm{d}\tilde{t}} = \frac{1}{\Theta Re}\left(\frac{1}{M^2}\tilde{\nabla}[\tilde{\nabla}\cdot\tilde{\boldsymbol{\omega}}] + \frac{1}{L^2}\tilde{\Delta}\tilde{\boldsymbol{\omega}} + \frac{2N^2}{(1-N^2)}\big[\tilde{\nabla}\times\tilde{\boldsymbol{v}} - 2\tilde{\boldsymbol{\omega}}\big]\right)\ , \end{aligned} \tag{28.7}$$

with the characteristic numbers

$$\begin{aligned} Re = \frac{\rho_0 v_{\mathrm{ref}}\ell_{\mathrm{ref}}}{\mu}\ , \quad L = \frac{\ell_{\mathrm{ref}}}{l}\ , \quad M = \frac{\ell_{\mathrm{ref}}}{m}\ , \quad N = \sqrt{\frac{\tau}{\mu+\tau}}\ , \\ \Theta = \frac{J_0}{\ell_{\mathrm{ref}}^2}\ , \quad l = \sqrt{\frac{\beta+\gamma}{\mu}}\ , \quad m = \sqrt{\frac{\alpha+\beta-\gamma}{\mu}}\ . \end{aligned} \tag{28.8}$$

Therein, $Re$ is the Reynolds number, $N$ is the coupling number, $L$, $M$ and $\Theta$ are characteristic length scale parameters. While all of the aforementioned parameters are dimensionless, the parameters $l$ and $m$ have the dimension of a length. Thus $L$ and $M$ are referred to as length scale parameters. Note that the parameters $N$ and $L$ are usually employed in context of Eringen's micropolar theory, see, *e.g.*, Cowin (1974); Rueger and Lakes (2016); Singh (1982), because they are characteristic for solutions of common flow problem such as Hagen-Poiseuille flow, *cf.* Cowin (1974), or Couette flow, see Eq. (28.14).

The coupling parameter $N$ may vary between zero and one, where the former corresponds to a vanishing influence of the mesoscopic scale and the latter represents a negligible macroscopic scale. Obviously, the limit value $N = 0$ can be achieved by considering an ordinary fluid. The case of $N = 1$, however, is a rather theoretical limit and only values smaller than one should be considered. The other length scale parameters such as $L$ and $M$ are positive numbers that may become infinite in the limit of a vanishing influence of the mesoscopic scale. In the other limit

of a strong influence they tend to zero but are always greater than zero, because the shear viscosity, $\mu$, does not vanish.

We proceed by employing the following two dimensional *ansatz* for the velocity and angular velocity to both problems:

$$\tilde{\boldsymbol{v}} = \tilde{v}_x(\tilde{x},\tilde{y})\boldsymbol{e}_x + \tilde{v}_y(\tilde{x},\tilde{y})\boldsymbol{e}_y \ , \quad \tilde{\boldsymbol{\omega}} = \tilde{\omega}(\tilde{x},\tilde{y})\boldsymbol{e}_z \ . \tag{28.9}$$

Note that the angular velocity field is solenoidal in the two-dimensional case and therefore the parameter $M$ is not present in the equations specialized for two-dimensional flows. The simplified dimensionless system reads:

$$\begin{aligned} \tilde{\nabla}\cdot\tilde{\boldsymbol{v}} = 0 \ , \quad \tilde{\boldsymbol{v}}\cdot(\tilde{\nabla}\otimes\tilde{\boldsymbol{v}}) &= -\tilde{\nabla}\tilde{p} + \frac{1}{(1-N^2)Re}\left(\tilde{\Delta}\tilde{\boldsymbol{v}} + 2N^2\tilde{\nabla}\times\tilde{\boldsymbol{\omega}}\right) \ , \\ \tilde{\boldsymbol{v}}\cdot(\tilde{\nabla}\tilde{\omega}) &= \frac{1}{\Theta Re}\left(\frac{1}{L^2}\tilde{\Delta}\tilde{\omega} + \frac{2N^2}{(1-N^2)}\left[(\tilde{\nabla}\times\tilde{\boldsymbol{v}})\cdot\boldsymbol{e}_z - 2\tilde{\omega}\right]\right) \ . \end{aligned} \tag{28.10}$$

In contrast to a Navier–Stokes fluid with the Reynolds number as a single characteristic parameter, there are four characteristic parameters for a micropolar fluid. For a discussion of the rough orders of magnitude of the dimensionless parameters in context with blood flow the reader is referred to Sect. 28.5.

### *28.3.2 Boundary Conditions and Boundary Value Problems*

For the statement of a complete problem, the equations presented above need to be supplemented by boundary conditions. For ordinary fluids physically correct boundary conditions seem to be "intuitively" clear, so that it is customary to impose (say) no-slip boundary conditions for the velocity at solid walls, because fluids usually stick to walls. It turns out, that this is neither intuitively clear nor always true. Although the historical review in Day (1990) strongly suggests, that the no-slip boundary condition is applicable in many flow situations, there are papers, *e.g.*, Brenner (2011); Lauga et al (2007), stating, that there are several mechanisms, which can lead to slip effects. Lauga et al (2007) state, that although there are different mechanisms for slip at fluid-solid interfaces, a distinction is of no practical importance. Furthermore, the so-called apparent slip length ranges over several orders of magnitude up to hundreds of nanometers. However, because usual (macroscopic) experiments are of much larger dimensions, the effect of slip is negligible such that no-slip boundary conditions at solid walls are reasonably applicable in many flow situations - at least as a first approximation.

Analogously the question of correct boundary conditions for the angular velocity in the theory of micropolar fluids is still under debate, see Alizadeh et al (2011); Hogan and Henriksen (1989); Kirwan (1986); Kolpashchikov et al (1983); Łukaszewicz (1999); Silber et al (2007). There are several suggestions of boundary conditions for the angular velocity at solid walls, but there is no convincing argu-

ment for one of them to be always preferable. Most of the suggested conditions can be categorized in three groups and may be referred to as follows:

- stick (or slip) controlled, where the angular velocity is prescribed due to the state of the wall (and the fluid) but independently of the velocity,
- vorticity controlled, where the angular velocity is proportional to the vorticity of the fluid near the wall, or
- force controlled, where the term *force* also refers to generalized forces and the angular velocity is influenced through forces and moments acting on the surface of the fluid.

While the first condition is analogous to the (say) no-slip condition of the velocity, the same comments as above apply for the angular velocity. Łukaszewicz (1999) refers to this boundary condition as "physically clear (the viscous fluid sticks to the solid boundary)." However, another study considers slip conditions and confirms them by molecular dynamic simulations, Chakraborty and Chakraborty (2008).

Another boundary condition commonly used is to assume that the angular velocity is proportional to the vorticity, Kirwan (1986); Kolpashchikov et al (1983); Hogan and Henriksen (1989). The reasoning behind this is, that the microstructure near solid walls needs to become irrelevant such that the angular velocity is solely given through the vorticity.

A third type of boundary conditions considers the coupling of angular velocity, vorticity and possible moment tractions at interfaces, Aero et al (1965); Łukaszewicz (1999). However, the correct choice of boundary conditions involving tractions is still under debate even for ordinary fluids, Sani and Gresho (1994). The same applies for micropolar fluids. Insights of how to impose angular velocity boundary conditions experimentally is given in none of the references mentioned above, see also Rickert et al (2018) for a discussion.

In this paper, only geometric boundary conditions directly applied on the velocity or angular velocity field are considered. Furthermore, we will impose only no-slip boundary conditions, because they are experimentally confirmed, Day (1990), at least for ordinary fluids.

In the Couette flow problem, two parallel plates of infinite extent are moving relatively to each other. The upper plate moves at a prescribed velocity $\boldsymbol{v} = v_0 \boldsymbol{e}_x$ while the bottom plate is at rest. The angular velocity is assumed to vanish at both plates, because they are manufactured in such a way not to induce any microrotation. In order to mimic Couette flow, periodic boundary conditions are employed. Hence, the boundary value problem is to solve Eqs. (28.10) subjected to the following boundary conditions:

$$\begin{cases} \tilde{\omega}(\tilde{\boldsymbol{x}}) = 0 \,, \quad \tilde{\boldsymbol{v}}(\tilde{\boldsymbol{x}}) = \boldsymbol{0} \,, & \tilde{\boldsymbol{x}} \in \Gamma_1 \,, \\ \tilde{\omega}(\tilde{\boldsymbol{x}}) = 0 \,, \quad \tilde{\boldsymbol{v}}(\tilde{\boldsymbol{x}}) = \boldsymbol{e}_x \,, & \tilde{\boldsymbol{x}} \in \Gamma_3 \,, \\ \tilde{\boldsymbol{v}}(\tilde{x} = 0, \tilde{y}) = \tilde{\boldsymbol{v}}(\tilde{x} = \ell/h, \tilde{y}) \,, & \\ \tilde{\omega}(\tilde{x} = 0, \tilde{y}) = \tilde{\omega}(\tilde{x} = \ell/h, \tilde{y}) \,, & 0 < \tilde{y} < 1 \,. \end{cases} \tag{28.11}$$

For the lid-driven cavity problem, it is also assumed that the angular velocity vanishes at the top. Furthermore, at all other boundaries the velocity and the angu-

lar velocity vanish. The complete boundary value problem consists of Eqs. (28.10) subjected to the following boundary conditions:

$$\begin{cases} \tilde{\omega}(\tilde{\boldsymbol{x}}) = 0 \,, & \tilde{\boldsymbol{v}}(\tilde{\boldsymbol{x}}) = \boldsymbol{e}_x \,, & \tilde{\boldsymbol{x}} \in \Gamma_3 \,, \\ \tilde{\omega}(\tilde{\boldsymbol{x}}) = 0 \,, & \tilde{\boldsymbol{v}}(\tilde{\boldsymbol{x}}) = \boldsymbol{0} \,, & \tilde{\boldsymbol{x}} \in (\Gamma_1 \cup \Gamma_2 \cup \Gamma_4) \,. \end{cases} \tag{28.12}$$

### *28.3.3 Reference Solution*

For the Couette flow, an analytical solution is given in Cowin (1974) and derived in Rickert et al (2018). Cowin (1974) uses a semi-inverse *ansatz* for the stationary solution:

$$\boldsymbol{v} = v(y)\boldsymbol{e}_x \,, \qquad \boldsymbol{\omega} = \omega(y)\boldsymbol{e}_z \,, \qquad p = p(y) \,, \tag{28.13}$$

for which the convective terms drop out. Hence, the resulting problem is linear and the following solution can be derived:

$$\begin{aligned} \frac{v(\tilde{y})}{v_0} &= \frac{1}{2(1-P)} \left[ 2\tilde{y} - P\left( 1 + \frac{\sinh(NL[2\tilde{y}-1])}{\sinh(NL)} \right) \right] , \\ \frac{\omega(\tilde{y})}{v_0/h} &= \frac{1}{2(1-P)} \left[ \frac{\cosh(NL[2\tilde{y}-1])}{\cosh(NL)} - 1 \right] , \quad P = \frac{N}{L} \tanh(NL) \,, \end{aligned} \tag{28.14}$$

where $\tilde{y} = y/h$ is the dimensionless vertical coordinate and for the dimensionless numbers $\ell_{\mathrm{ref}} = h$ is applied. The solution does not depend on the parameter $\Theta$, which describes the influence of the microinertia.

## 28.4 Numerical Treatment

We solve the resulting set of dimensionless partial differential equations (28.10) using the finite element method. A spatial discretization based on the stable $P_2$-$P_1$ Taylor-Hood element for velocity and pressure is employed, Taylor and Hood (1973). The scalar angular velocity is discretized using a $P_1$ element. We describe the derivation of the weak form for both of the proposed problems in the Appendix.

The FEniCS library, Alnæs et al (2015); Logg et al (2012), as applied for many problems in continuum mechanics (Abali, 2017), allows to solve the finite element problem once the weak form is implemented. The discrete weak form represents a set of nonlinear algebraic equations, which is commonly solved using Newton's method. However, for our stationary problem, there is no appropriate initial guess available. Due to this fact, the solution procedure is altered and based on a hybrid approach possessing a larger convergence radius (Elman et al, 2006). This hybrid approach first performs a Picard iteration and as a second step applies Newton's

method. The main difference between the two steps lies in the linearization of the convective term, see Elman et al (2006).

The parameter study requires a series of subsequent simulations and while one parameter is varied, we use the previous solution as the initial guess. This reduces the number of iterations required. In this sense, our method can also be regarded as a continuation method. Nevertheless, we tested the hybrid approach without parameter continuation and the simulations converged over the entire range of tested parameters.

### *28.4.1 Convergence Analysis*

In order to verify the implemented finite element code, we perform a convergence analysis based on the analytical solution of the Couette flow problem. The set of nominal values for the dimensionless parameters given in Sec. 28.5 is used. The error of the numerical solution obtained from the finite element program w.r.t. the analytical solution is computed using the following error measures:

$$e^{\mathrm{abs}}(\psi) = \frac{\int_V \|\psi^{\mathrm{ana}} - \psi^{\mathrm{num}}\| \, \mathrm{d}V}{\int_V \mathrm{d}V} \,, \quad e^{\mathrm{rel}}(\psi) = \frac{\int_V \|\psi^{\mathrm{ana}} - \psi^{\mathrm{num}}\| \, \mathrm{d}V}{\int_V \|\psi^{\mathrm{ana}}\| \, \mathrm{d}V} \,, \tag{28.15}$$

where the $\|\cdot\|$ is the absolute value if $\psi$ is a scalar and the Eulidean norm if $\psi$ is a vector. Here, $e^{\mathrm{abs}}$ and $e^{\mathrm{rel}}$ refer to the absolute and relative error respectively. Furthermore, $\psi^{\mathrm{ana}}$ and $\psi^{\mathrm{num}}$ denote the analytical and the numerical solution, respectively. A series of simulations on globally refined meshes is performed and the fineness of the mesh is characterized by the number of nodes, $n$, in the vertical direction of the channel ($\boldsymbol{e}_y$ direction). Although the mesh is not successively refined, the aspect ratio of the elements remains constant in the refinement process, which ensures that the quality of the elements is not deteriorated.

Figure 28.2 shows the results of the convergence analysis. The errors for the velocity (Fig. 28.2a) as well as for the angular velocity (Fig. 28.2b) decrease monotonically for the relative and the absolute error as the number of nodes is increased. Both regression lines have a slope of $-2$ in the double logarithmic chart, which indicates that the method is of second order. In conclusion, our finite element implementation to simulate the stationary flow of a micropolar fluid is convergent and therefore it is considered as a reliable tool to assess the influence of the model parameters in more complex flow situations. The largest number of nodes in the vertical direction applied in the convergence analysis is $800$, which corresponds to $645\,284$ degrees of freedom in total.

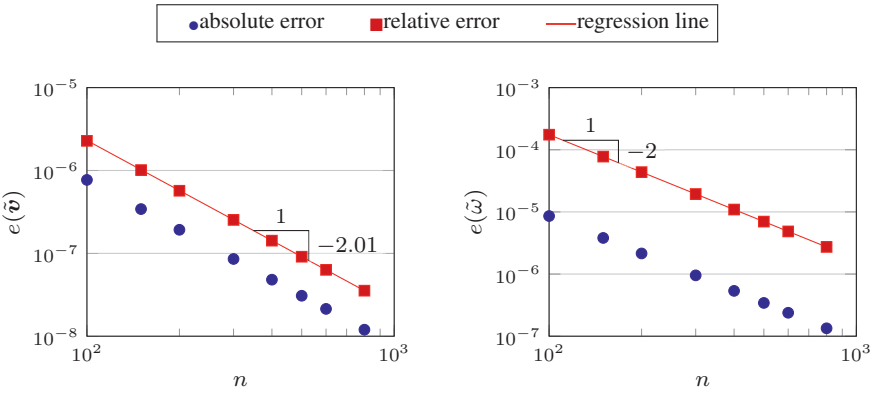


**(a)** Errors w.r.t. the velocity field.

**(b)** Errors w.r.t. the angular velocity field.

**Fig. 28.2** Convergence results for the Couette flow problem. The legend above applies for both diagrams.

## 28.5 Results and Discussion

In this section, the results of the parameter study for the lid-driven cavity problem shown in Fig. 28.1b are presented. The computations are performed on an equidistant grid using 100 points in horizontal and vertical direction. For the parameter analysis a set of nominal values is selected and only one parameter at a time is varied in a given range. The following nominal values are chosen: $Re = 200$, $L = 0.4$, $N = 0.25$, and $\Theta = 10^{-9}$. This choice as well as the parameter ranges will be motivated by the following considerations.

In context of blood flow with a viscosity of $\mu = 3 \times 10^{-3}\,\mathrm{kg\,m^{-1}\,s^{-1}}$ to $4 \times 10^{-3}\,\mathrm{kg\,m^{-1}\,s^{-1}}$ (Popel and Pittman, 2000), the nominal Reynolds number corresponds to a mean velocity of $5.6 \times 10^{-2}\,\mathrm{m\,s^{-1}}$ to $7.6 \times 10^{-2}\,\mathrm{m\,s^{-1}}$ for a reference length of 1 cm. If the reference length is 1 mm, the mean velocity ranges from $5.6 \times 10^{-1}\,\mathrm{m\,s^{-1}}$ to $7.6 \times 10^{-1}\,\mathrm{m\,s^{-1}}$. Comparing these values with the ones given in Lieber (2000) suggests that the Reynolds number is slightly too high when considering arterioles. However, blood flow is not stationary and the Reynolds number, which depends on the type of the blood vessel and ranges from approx. 0.005 to 7000, exceeds six orders of magnitude (Caro et al, 2012). Therefore, the Reynolds number is varied over a large range in this study.

Based on the viscosities for human blood specified in Kang and Eringen (1976) and Papautsky et al (1999), $N = 0.25$ and $L = 0.4$ is obtained as a rough estimate for a reference length of 1 cm. The length scale parameter $L$ decreases linearly, if the reference length decreases, but it strongly depends upon the viscosities and may therefore vary over a larger range. In order to obtain an estimate for $\Theta$, erythrocytes are considered as a principle of component of blood. Applying $\ell_{\mathrm{ref}} = 0.1\,\mathrm{mm}$ to 1 mm for the diameter of small arteries or terminal branches (Schneck, 2000), and $d \approx 7.5\,\mu\mathrm{m}$ for the diameter of erythrocytes, Schneck (2000), gives $J_0 \approx 10^{-12}\,\mathrm{m^2}$

and $\Theta = 10^{-6}$ to $10^{-5}$. This number would of course increase to $10^{-2}$ for arterioles ($d < 100\,\mu\text{m}$) or even to 1 for capillaries ($d < 10\,\mu\text{m}$), see Schneck (2000).

In view of the facts outlined above, the Reynolds number is varied from the $0.01$ to $5000$. The coupling parameter $N$ is varied from $0$ to $0.95$. The length scale $L$ is varied from $10^{-3}$ to $10^{2}$, where the latter represents a rather extreme case. Finally, the parameter $\Theta$ characterizing microinertia is varied from $10^{-9}$ to $1$.

### *28.5.1 Vertical and Horizontal Profiles*

The results are presented by using line plots of the velocity and angular velocity along the vertical and horizontal middle lines of the cavity, see dashed lines in Figs. 28.3. In Fig. 28.3a an example of the streamline of the flow of an ordinary Navier–Stokes fluid is given. There is a main eddy located close to the center and two so-called Moffatt eddies are present at the two bottom corners, Moffatt (1964). The eddy structure of this problem was explored in detail for Navier–Stokes fluids. It was shown that another eddy occurs close to the top-left corner and secondary corner eddies are present for higher Reynolds numbers (Shankar, 1993; Shen, 1991).

Figures 28.4 and 28.5 show the profiles for varying values of $N$. Considering the horizontal and vertical profiles of the angular velocity, it is evident that the larger the value of $N$ the larger the amplitudes of the angular velocity. The angular velocity is mainly negative along the horizontal and vertical profile for small to moderate values of $N$. There are small domains at the boundaries, where the angular velocity is positive.[3] These domains grow for large values of $N$. This suggests that the parameter $N$ gradually changes the spatial structure of the angular velocity field, whereas the qualitative behavior is not altered. The influence of the parameter $N$ on the velocity profiles is not so strong when compared to the angular velocity. Slight changes are visible, which are more prominent in the vertical profile.

Figures 28.6 and 28.7 show the profiles for varying values of $L$. In the profiles of the angular velocity the formation of a very thin boundary layer is visible—the larger $L$ the thiner the boundary layer. The boundary layer is most prominent at the top of the cavity, whereas there is no layer at the bottom. At the left and right walls, boundary layers are also present. Although the amplitudes differ only by an order of magnitude compared to those obtained for large values of $N$, the qualitative structure of the profiles for the angular velocity is very different when $L$ is varied. Comparing the angular velocity profiles for varying $L$ among each other shows, that apart from a scaling a marginal shift in the spatial structure is visible. The zero crossings move gradually, if $L$ varies. For the influence of the parameter $L$ on the velocity profiles, the same applies as for the parameter $N$—a significant change was not observed.

Figures 28.8 and 28.9 show the profiles for varying values of $Re$. Increasing the Reynolds number above approximately $100$ results in changes of the velocity

[3] These domains are not really visible due to the scaling.

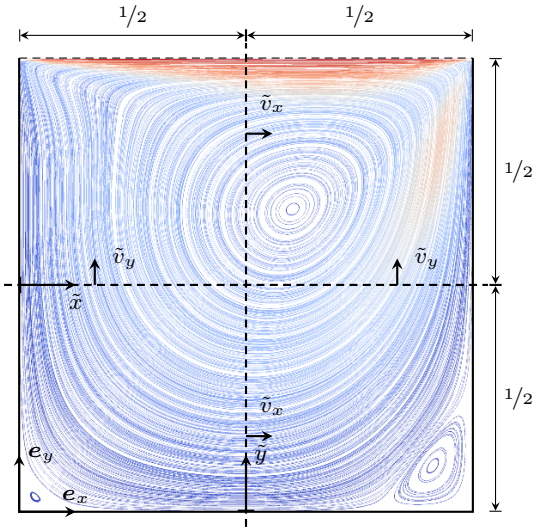


**(a)** Streamline plot with dashed lines for profiles.

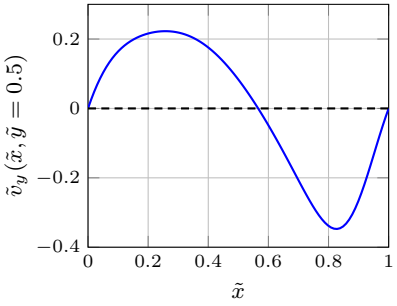


**(b)** Velocity profile along $\tilde{x}$-axis.

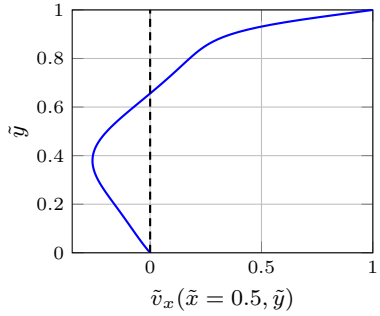


**(c)** Velocity profile along $\tilde{y}$-axis.

**Fig. 28.3** Streamlines (a) and profiles of the velocity (b, c) for the lid-driven cavity problem of a Navier–Stokes fluid with $Re = 200$. Color indicates the magnitude of the velocity.

profiles. If the Reynolds number is below approximately 10, the profiles of the velocity are identical for the horizontal and vertical direction regardless of the value of $Re$. The same holds true for the angular velocity. At higher Reynolds numbers, a boundary layer develops and the center of the main vortex (zero crossing of the velocity in the vertical profile) moves downwards. Regarding the vertical profiles, there is a correlation of the angular velocity with the velocity—the minimum of the angular velocity is roughly located where the velocity is zero. This effect is also visible in the right inset of Fig. 28.8 in terms of a decrease of the angular velocity at $\tilde{x} \approx 0.5$ for $Re \geq 200$. We stress that this decrease is not due to a change of the underlying solution because the angular velocity is linked to the velocity field

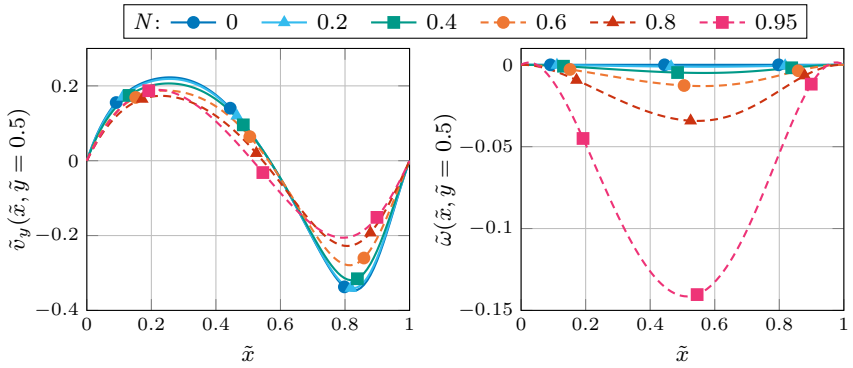


**Fig. 28.4** Horizontal profiles of the velocity and angular velocity for different values of $N$. The other parameters $Re$, $L$, and $\Theta$ have nominal values.

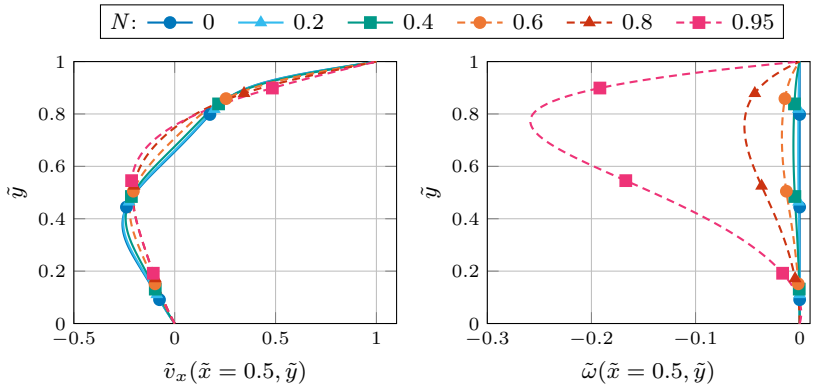


**Fig. 28.5** Vertical profiles of the velocity and angular velocity for different values of $N$. The other parameters $Re$, $L$, and $\Theta$ have nominal values.

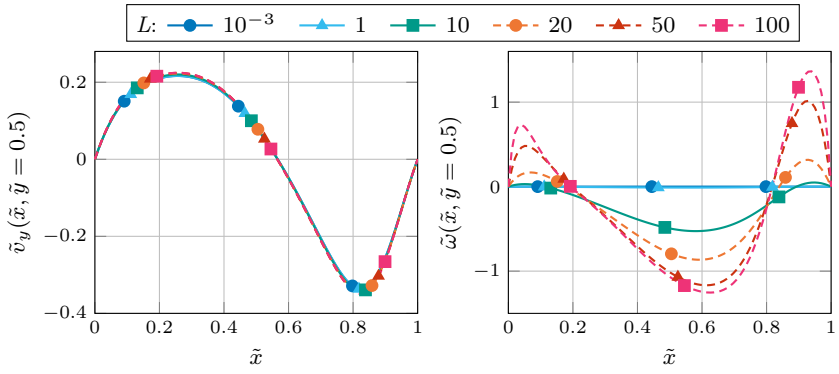


**Fig. 28.6** Horizontal profiles of the velocity and angular velocity for different values of $L$. The other parameters $Re$, $N$, and $\Theta$ have nominal values.

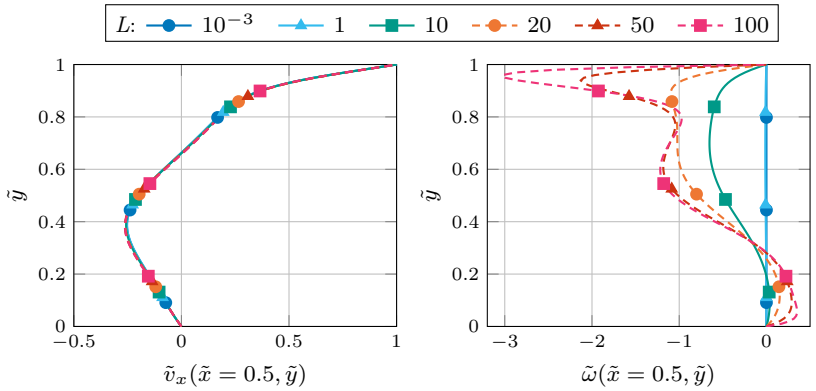


**Fig. 28.7** Vertical profiles of the velocity and angular velocity for different values of $L$. The other parameters $Re$, $N$, and $\Theta$ have nominal values.

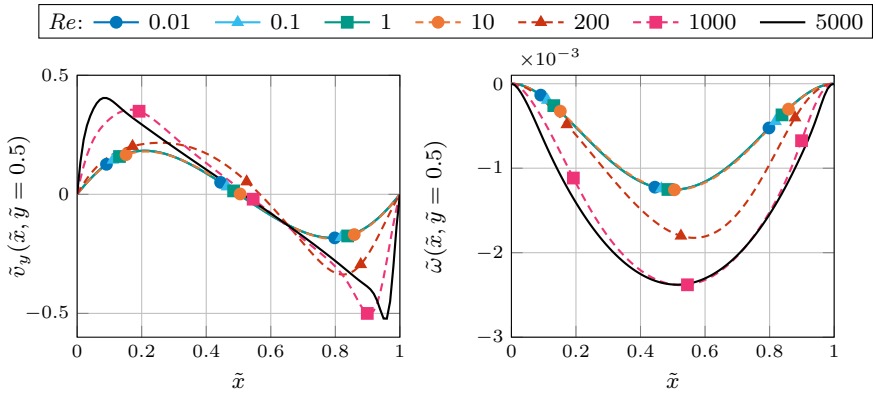


**Fig. 28.8** Horizontal profiles of the velocity and angular velocity for different values of $Re$. The other parameters $L$, $N$, and $\Theta$ have nominal values.

for chosen set of parameters. Finally, note that the angular velocity in Figs. 28.8 and 28.9 is three orders of magnitudes smaller than for example in Figs. 28.6 and 28.7.

The last parameter, which was varied, is the microinertia parameter $\Theta$. An influence of the microinertia parameter was not observed in the velocity field for the set of nominal values chosen in this study. This is expected because $\Theta$ is not present in the balance of linear momentum. The angular velocity field is also not significantly altered for small and moderate values of $\Theta$.

In summary, the approach of varying one parameter while the others parameter keep their nominal values has shown that the microinertia has the smallest effect on the structure of the solution. However, this is only true for the considered case and parameter set. The velocity field changes the most, if the Reynolds number is increased. But smaller alterations are also observable in the velocity field, if the

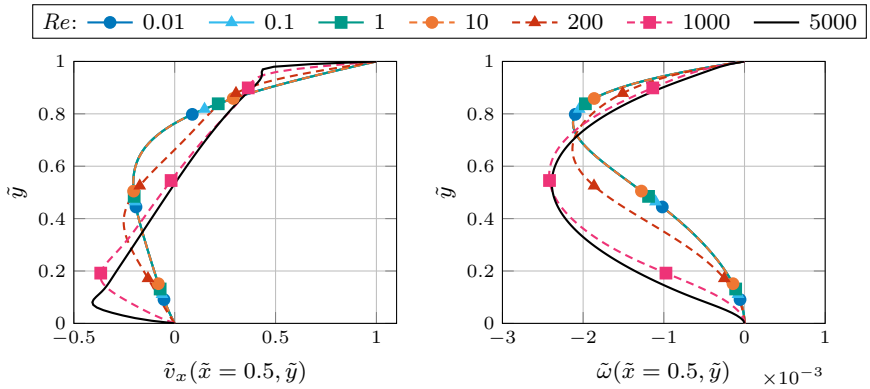


**Fig. 28.9** Vertical profiles of the linear and angular velocity for different values of $Re$. The other parameters $L$, $N$, and $\Theta$ have nominal values.

micropolar viscosity parameters $L$ and $N$ are changed. The micropolar viscosity parameters $L$ and $N$ both yield to the changes in the angular velocity field. The largest amplitudes associated with these parameters are approximately $0.3$ and $3$ respectively. In a broad sense, the parameter $N$ scales the solution, whereas increasing values of the parameter $L$ result in a stronger boundary layer.

### *28.5.2 Analysis of the Angular Velocity Field*

Figure 28.10 shows the angular velocity for a representative selection of parameters combinations. In Figs. 28.10a and 28.10b, the microrotation is confined to the top layer of the cavity and the spatial structure is strongly connected to the velocity field, see Fig. 28.3a. Comparing Figs. 28.10a to 28.10b suggests that the region at the top gets wider and thiner if $N$ is increased. In Figs. 28.10c and 28.10d, boundary layers become apparent. They are strongest close to the top-right corner of the cavity and the angular velocity penetrates deeper regions of the cavity.

An explanation might be that for the considered parameter set the convective term in Eq. $(28.10)_3$ can be dropped because the product $\Theta Re$ is small. This gives the following spin balance:

$$\frac{1}{L^2}\tilde{\Delta}\tilde{\omega} + \frac{2N^2}{(1-N^2)}\left[(\tilde{\nabla}\times\tilde{\boldsymbol{v}})\cdot\boldsymbol{e}_z - 2\tilde{\omega}\right] = 0\,, \tag{28.16}$$

which is interpreted as a Helmholtz equation for $\tilde{\omega}$ with the source term $\tilde{\nabla}\times\tilde{\boldsymbol{v}}$. If the parameter $L$ is large, the diffusive term is negligible because the factor $N^2/(1-N^2)$ is of order 1 for $N < 0.9$. In the limit, we can make the approximation $\tilde{\omega} \approx (\tilde{\nabla}\times\tilde{\boldsymbol{v}})/2\cdot\boldsymbol{e}_z$, which means that the angular velocity $\tilde{\omega}$ is directly coupled to the vorticity. This approximation was roughly confirmed for $L = 50$ by comparing the

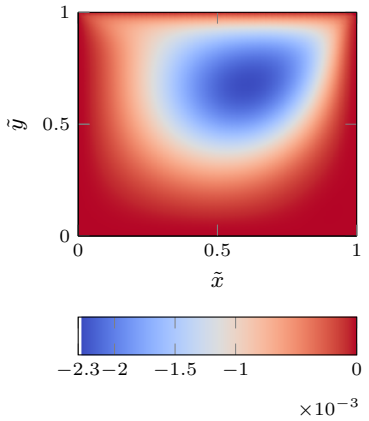


**(a)** $N = 0.25$, $L = 0.4$.

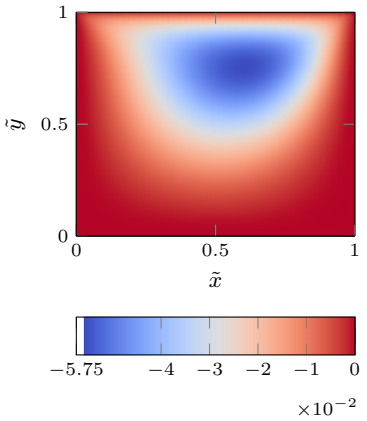


**(b)** $N = 0.8$, $L = 0.4$.

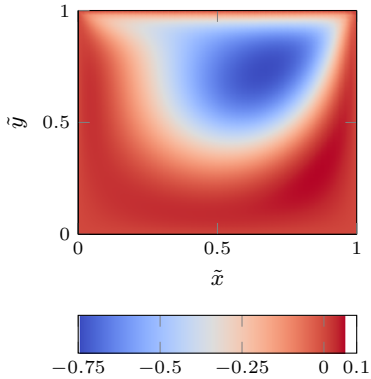


**(c)** $N = 0.25$, $L = 10$.

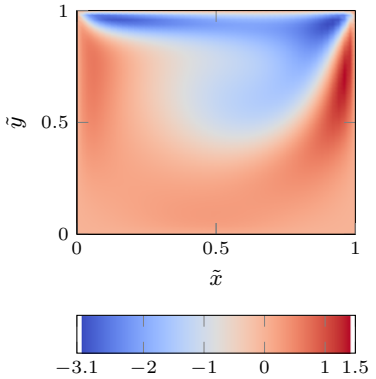


**(d)** $N = 0.25$, $L = 50$.

**Fig. 28.10** Angular velocity field $\tilde{\omega}$ for different values of $N$ and $L$. The other parameters have nominal values.

spatial structure of the angular velocity field with the one of the vorticity using our numerical results. However, for moderate values of $L$, the terms governed by the coupling parameter $N$ are balanced with the diffusion term. This seems to weaken the coupling mechanism because strong gradients close to the walls and corners are smoothed by diffusion. In conclusion, the findings suggest the dominant parameter for the lid-driven cavity problem is the micropolar viscosity parameter $L$.

## 28.6 Conclusion

This paper presents a parameter study of a micropolar fluid in a lid-driven cavity using the nominal values: $Re = 200$, $L = 0.4$, $N = 0.25$, and $\Theta = 10^{-9}$, which were discussed in context with the example of blood flow. Based on our results, we find that for the lid-driven cavity flow problem:

- The Reynolds number has the strongest effect on the velocity field and only influences the angular velocity by enhanced convective transport to lower regions. The observed effects are analogous to the results for a Navier–Stokes fluid.
- The microviscosity parameters $L$ and $N$ govern the coupling mechanism between velocity and angular velocity. Their influence on the velocity is rather weak but strong regarding the angular velocity. For the both parameters, the angular velocity is confined in the top half of the cavity. Especially, the parameter $L$ was identified as the one responsible for the formation of thin boundary layers close to the top-right corner.
- By scaling arguments, we explained the role of the parameter $L$ in the spin balance for the considered case. We showed that low values of $L$ smooth the solution for the angular velocity, whose source is located at regions of large velocity gradients, *e.g.*, at boundary layers. The larger $L$ the less the diffusivity and the more is the angular velocity confined to these boundary layers.
- The microinertia parameter $\Theta$ has almost no influence on the results. Only very large values of $\Theta$ lead to visible alterations in the angular velocity field.

Our study points to several aspects, which could be addressed in future work. First, we have only varied one parameter at a time, which limits us to lines in the parameter space. A full coverage of the parameter space allows to fully explore the mutual influence of the parameters. Secondly, stationary solutions were computed, which may be not be stable at all. Because of this, a stability analysis should be performed by either integrating the equations in time using the precomputed stationary solution as an initial condition or by performing a linear perturbation analysis. Third, the example of buoyancy driven flow in the cavity should be studied to further explore the impact of the parameters identified in this study. This could also incorporate microstructural changes due to temperature or pressure fluctuations, which were proposed in Müller and Vilchevskaya (2017).

## Appendix: Weak Forms

For the finite element formulation of Eqs. (28.10), weak forms of the differential equations need to be derived. Subsequently, the following short hand notation for inner products in the volume and on the boundary will be applied:

$$\left(\boldsymbol{A},\boldsymbol{B}\right)_{\Omega} = \int\limits_{\Omega} \boldsymbol{A} \star \boldsymbol{B}\,\mathrm{d}V\ , \quad \left\langle \boldsymbol{A},\boldsymbol{B}\right\rangle_{\Gamma} = \int\limits_{\Gamma} \boldsymbol{A} \star \boldsymbol{B}\,\mathrm{d}A\ ,$$

where $\boldsymbol{A} \star \boldsymbol{B}$ represents the contraction of two tensors $\boldsymbol{A}$ and $\boldsymbol{B}$ of arbitrary rank to a scalar. Here, $\Omega$ denotes the domain of integration with the boundary $\Gamma = \partial\Omega$. With the help of the operators

$$\begin{aligned}
\mathcal{A}(\boldsymbol{\phi}, \boldsymbol{\psi}) &= \big(\tilde{\nabla} \otimes \boldsymbol{\phi}, \tilde{\nabla} \otimes \boldsymbol{\psi}\big)_\Omega, \qquad \mathcal{B}(\boldsymbol{\phi}, \psi) = \big(\tilde{\nabla} \cdot \boldsymbol{\phi}, \psi\big)_\Omega, \\
\mathcal{C}(\boldsymbol{\phi}, \boldsymbol{\psi}) &= \big(\tilde{\boldsymbol{v}} \cdot (\tilde{\nabla} \otimes \boldsymbol{\phi}), \boldsymbol{\psi}\big)_\Omega, \quad \mathcal{D}_\Gamma(\boldsymbol{\phi}, \boldsymbol{\psi}) = \big\langle \boldsymbol{\phi}, \boldsymbol{\psi} \times \boldsymbol{e}_z \big\rangle_\Gamma, \\
\mathcal{D}(\phi, \boldsymbol{\psi}) &= \big(\phi, \tilde{\nabla} \cdot (\boldsymbol{\psi} \times \boldsymbol{e}_z)\big)_\Omega = \Big(\phi, \frac{\partial \psi_y}{\partial x} - \frac{\partial \psi_x}{\partial y}\Big)_\Omega,
\end{aligned}$$

a multiplication of Eqs. (28.10) with test functions $\delta p$, $\delta \boldsymbol{v}$, $\delta\omega$, $\delta J$ and subsequent integration over the (dimensionless) domain gives rise to the following weak forms:

$$\begin{aligned}
&\mathcal{B}(\tilde{\boldsymbol{v}}, \delta p) = 0 \,, \\
&\mathcal{C}(\tilde{\boldsymbol{v}}, \delta \boldsymbol{v}) = \mathcal{B}(\delta \boldsymbol{v}, \tilde{p}) - \big\langle \tilde{p}\boldsymbol{n}, \delta \boldsymbol{v} \big\rangle_\Gamma + \frac{2N^2}{(1-N^2)Re}\Big\{ \mathcal{D}(\tilde{\omega}, \delta \boldsymbol{v}) - \mathcal{D}_\Gamma(\tilde{\omega}\boldsymbol{n}, \delta \boldsymbol{v}) \Big\} + \\
&\qquad + \frac{1}{(1-N^2)Re}\Big\{ \big\langle \boldsymbol{n} \cdot (\tilde{\nabla} \otimes \tilde{\boldsymbol{v}}), \delta \boldsymbol{v} \big\rangle_\Gamma - \mathcal{A}(\tilde{\boldsymbol{v}}, \delta \boldsymbol{v}) \Big\} \,, \\
&\mathcal{C}(\tilde{\omega}, \delta\omega) = \frac{1}{L^2 \Theta Re}\Big( \big\langle \boldsymbol{n} \cdot (\tilde{\nabla}\tilde{\omega}), \delta\omega \big\rangle_\Gamma - \mathcal{A}(\tilde{\omega}, \delta\omega) \Big) + \\
&\qquad + \frac{2N^2}{(1-N^2)\Theta Re}\Big( \mathcal{D}(\delta\omega, \tilde{\boldsymbol{v}}) - 2\big(\tilde{\omega}, \delta\omega\big)_\Omega \Big).
\end{aligned}$$

For the lid-driven cavity problem, pure Dirichlet boundary conditions are considered in form of no-slip conditions for both the velocity and angular velocity. In this case, the test functions $\delta p$, $\delta \boldsymbol{v}$ and $\delta\omega$ vanish at the boundary and therefore all boundary terms vanish. Hence, the simplified weak forms can be written as:

$$\begin{aligned}
&\mathcal{B}(\tilde{\boldsymbol{v}}, \delta p) = 0 \,, \\
&\mathcal{C}(\tilde{\boldsymbol{v}}, \delta \boldsymbol{v}) = \mathcal{B}(\delta \boldsymbol{v}, \tilde{p}) - \frac{1}{(1-N^2)Re}\Big( \mathcal{A}(\tilde{\boldsymbol{v}}, \delta \boldsymbol{v}) - 2N^2 \mathcal{D}(\tilde{\omega}, \delta \boldsymbol{v}) \Big) \,, \\
&\mathcal{C}(\tilde{\omega}, \delta\omega) = \frac{1}{\Theta Re}\left[ \frac{2N^2}{(1-N^2)}\Big( \mathcal{D}(\delta\omega, \tilde{\boldsymbol{v}}) - 2\big(\tilde{\omega}, \delta\omega\big)_\Omega \Big) - \frac{1}{L^2}\mathcal{A}(\tilde{\omega}, \delta\omega) \right] .
\end{aligned}$$

The same holds for the Coutte flow except for the periodic boundaries $\Gamma_2$ and $\Gamma_4$. The surface integral related to the pressure, $p$, vanishes due to periodicity. The pressure gradient has the same values at $\Gamma_2$ and $\Gamma_4$, but the normal vectors have a different direction, *i.e.*, $\boldsymbol{n}_{\Gamma_2} = -\boldsymbol{n}_{\Gamma_4}$. Therefore, the simplified weak forms for the Couette flow can be expressed as:

$$
\begin{aligned}
&\mathcal{B}(\tilde{\boldsymbol{v}}, \delta p) = 0 \,, \\
&\mathcal{C}(\tilde{\boldsymbol{v}}, \delta \boldsymbol{v}) = \mathcal{B}(\delta \boldsymbol{v}, \tilde{p}) + \frac{2N^2}{(1-N^2)Re} \mathcal{D}(\tilde{\omega}, \delta \boldsymbol{v}) + \\
&\qquad\qquad + \frac{1}{(1-N^2)Re} \Big\{ \big\langle \boldsymbol{n} \cdot (\tilde{\nabla} \otimes \tilde{\boldsymbol{v}}), \delta \boldsymbol{v} \big\rangle_{\Gamma} - \mathcal{A}(\tilde{\boldsymbol{v}}, \delta \boldsymbol{v}) \Big\} \,, \\
&\mathcal{C}(\tilde{\omega}, \delta \omega) = \frac{1}{L^2 \Theta Re} \Big( \big\langle \boldsymbol{n} \cdot (\tilde{\nabla} \tilde{\omega}), \delta \omega \big\rangle_{\Gamma} - \mathcal{A}(\tilde{\omega}, \delta \omega) \Big) + \\
&\qquad\qquad + \frac{2N^2}{(1-N^2)\Theta Re} \Big( \mathcal{D}(\delta \omega, \tilde{\boldsymbol{v}}) - 2 \big(\tilde{\omega}, \delta \omega\big)_{\Omega} \Big).
\end{aligned}
$$

## References


Abali BE (2017) Computational Reality, 1st edn. Advanced Structured Materials, Springer

Aero EL, Bulygin AN, Kuvshinskii EV (1965) Asymmetric hydromechanics. Journal of Applied Mathematics and Mechanics 29(2):333–346

Alizadeh M, Silber G, Nejad AG (2011) A continuum mechanical gradient theory with an application to fully developed turbulent flows. Journal of Dispersion Science and Technology 32(2):185–192

Alnæs MS, Blechta J, Hake J, Johansson A, Kehlet B, Logg A, Richardson C, Ring J, Rognes ME, Wells GN (2015) The fenics project version 1.5. Archive of Numerical Software 3(100)

Anders D, Weinberg K (2011) A variational approach to the decomposition of unstable viscous fluids and its consistent numerical approximation. ZAMM—Journal of Applied Mathematics and Mechanics / Zeitschrift für Angewandte Mathematik und Mechanik 91(8):609–629

Ariman T, Turk M, Sylvester N (1973) Microcontinuum fluid mechanic—A review. International Journal of Engineering Science 11(8):905–930

Aydin O, Pop I (2007) Natural convection in a differentially heated enclosure filled with a micropolar fluid. International Journal of Thermal Sciences 46(10):963–969

Botella O, Peyret R (1998) Benchmark spectral results on the lid-driven cavity flow. Computers & Fluids 27(4):421–433

Bourantas G, Loukopoulos V (2014) Modeling the natural convective flow of micropolar nanofluids. International Journal of Heat and Mass Transfer 68:35–41

Brenner H (2011) Beyond the no-slip boundary condition. Physical Review E 84(4):0463,091–8

Bruneau CH, Saad M (2006) The 2d lid-driven cavity problem revisited. Computers & Fluids 35(3):326–348

Caro CG, Pedley TJ, Schroter RC, Seed WA (2012) The mechanics of the circulation., 2nd edn. Cambridge University Press

Chakraborty D, Chakraborty S (2008) Towards a generalization of hydrodynamic boundary conditions for flows of fluids with homogeneous internally rotating structures. Physics Letters A 372(33):5462–5466

Chakravarthy V, Ottino J (1996) Mixing of two viscous fluids in a rectangular cavity. Chemical Engineering Science 51(14):3613–3622

Cortes AB, Miller JD (1994) Numerical experiments with the lid driven cavity flow problem. Computers & Fluids 23(8):1005–1027

Cowin SC (1974) The theory of polar fluids. In: Yih CS (ed) Advances in Applied Mechanics, vol. 14, Academic Press, Inc., New York, pp 279–347

Day MA (1990) The no-slip condition of fluid dynamics. Erkenntnis 33(3):285–296

Elman H, Silvester D, Wathen A (2006) Finite Elements and Fast Iterative Solvers: with Application in Incompressible Fluid Dynamics, Numerical Mathematics and Scientific Computation, vol 1. Oxford University Press

Eringen AC (1964) Simple microfluids. International Journal of Engineering Science 2(2):205–217

Eringen AC (1966) Theory of micropolar fluids. Journal of Mathematics and Mechanics 16(1):1–18

Eringen AC (1985) Rigid suspensions in viscous fluid. International Journal of Engineering Science 23(4):49–495

Eringen AC (1991) Continuum theory of dense rigid suspensions. Rheologica Acta 30(1):23–32

Eringen AC (2001) Microcontinuum Field Theories- II Fluent Media. Springer, Berlin, Heidelberg, New York

Erturk E, Gökccöl C (2008) Fourth-order compact formulation of navier-stokes equations and driven cavity flow at high reynolds numbers. International Journal for Numerical Methods in Fluids 50(4):421–436

Freitas CJJ, Street RL, Findikakis AN, Koseff JR (1985) Numerical simulation of three-dimensional flow in a cavity. International Journal for Numerical Methods in Fluids 5(6):561–575

Gibanov NS, Sheremet MA, Pop I (2016a) Free convection in a trapezoidal cavity filled with a micropolar fluid. International Journal of Heat and Mass Transfer 99:831–838

Gibanov NS, Sheremet MA, Pop I (2016b) Natural convection of micropolar fluid in a wavy differentially heated cavity. Journal of Molecular Liquids 221:518–525

Glane S, Rickert W, Müller WH, Vilchevskaya E (2017) Micropolar media with structural transformations: Numerical treatment of a particle crusher. In: Advanced problems in mechanics/ Proceedings of the XLV Summer school-conference, Russian Academy of Sciences, Institute for Problems in Mechanical Engineering, Peter the Great St.Petersburg Polytechnic University, pp 197–211

Hogan HA, Henriksen M (1989) An evaluation of a micropolar model for blood flow through an idealized stenosis. Journal of Biomechanics 22(3):211–218

Hsu TH, Chen CK (1996) Natural convection of micropolar fluids in a rectangular enclosure. International Journal of Engineering Science 34(4):407–415

Iwatsu R, Hyun JM (1995) Three-dimensional driven-cavity flows with a vertical temperature gradient. International Journal of Heat and Mass Transfer 38(18):3319–3328

Jena SK, Bhatacharyya SP (1986) The effect of microstructure on the thermal convection in a rectangular box of fluid heated from below. International Journal of Engineering Science 24(1):69–78

Kang CK, Eringen AC (1976) The effect of microstructure on the rheological properties of blood. Bulletin of Mathematical Biology 38(2):135–159

Kareem AK, Gao S, Ahmed AQ (2016) Unsteady simulations of mixed convection heat transfer in a 3d closed lid-driven cavity. International Journal of Heat and Mass Transfer 100:121–130

Kirwan AD (1986) Boundary conditions for micropolar fluids. International Journal of Engineering Science 24(7):1237–1242

Kolpashchikov VL, Migun NP, Prokhorenko PP (1983) Experimental determination of material micropolar fluid constants. International Journal of Engineering Science 21(4):405–411

Lauga E, Brenner M, Stone H (2007) Microfluidics: The no-slip boundary condition. In: Tropea C, Yarin AL, Foss JF (eds) Springer Handbook of Experimental Fluid Mechanics, Springer, Berlin, Heidelberg, New York, pp 1219–1240

Le Quere P, Humphrey JAC, Sherman FS (1981) Numerical calculation of thermally driven two-dimensional unsteady laminar flow in cavities of rectangular cross section. Numerical Heat Transfer 4(3):249–283

Lieber BB (2000) Arterial Macrocirculatory Hemodynamics. In: Bronzino JD (ed) The Biomedical Engineering Handbook, vol 1, 2nd edn, CRC Press, chap 30

Logg A, Wells GN, Hake J (2012) DOLFIN: a C++/Python Finite Element Library, Springer, chap 10, pp 173–225

Łukaszewicz G (1999) Micropolar fluids: Theory and applications. Springer Science & Business Media

Maugin GA (2011) A Historical Perspective of Generalized Continuum Mechanics. In: Altenbach H, Maugin GA, Erofeev V (eds) Mechanics of Generalized Continua, Springer, Berlin, Heidelberg, chap 1, pp 3–19

Moffatt HK (1964) Viscous and resistive eddies near a sharp corner. Journal of Fluid Mechanics 18(1):1–18

Müller WH, Vilchevskaya EN (2017) Micropolar theory from the viewpoint of mesoscopic and mixture theories. Physical Mesomechanics 20(3):263–279

Müller WH, Vilchevskaya EN (2018) Micropolar theory with production of rotational inertia: A rational mechanics approach. In: Altenbach H, Pouget J, Rousseau M, Collet B, Michelitsch T (eds) Generalized Models and Non-classical Approaches in Complex Materials 1, Advanced Structured Materials, Springer International Publishing, pp 581–606

Müller WH, Vilchevskaya EN, Weiss W (2017) Micropolar theory with production of rotational inertia: A farewell to material description. Physical Mesomechanics 20(3):250–262

Nallasamy M, Prasad KK (1977) On cavity flow at high reynolds numbers. Journal of Fluid Mechanics 79(2):391–414

Papautsky I, Brazzle J, Ameel T, Frazier AB (1999) Laminar fluid behavior in microchannels using micropolar fluid theory. Sensors and Actuators A: Physical 73(1-2):101–108

Popel AS, Pittman RN (2000) Mechanics and Transport in the Microcirculation. In: Bronzino JD (ed) The Biomedical Engineering Handbook, vol 1, 2nd edn, CRC Press, chap 31

Prakash J, Sinha P (1975) Lubrication theory for micropolar fluids and its application to a journal bearing. International Journal of Engineering Science 13(3):217–232

Rickert W, Müller WH, Vilchevskaya EN (2018) A note on couette flow of micropolar fluids according to eringen's theory. Mathematics and Mechanics of Complex Systems Submitted

Rueger Z, Lakes RS (2016) Experimental cosserat elasticity in open-cell polymer foam. Philosophical Magazine 96(2):93–111

Sani RL, Gresho PM (1994) Résumé and remarks on the open boundary condition minisymposium. International Journal for Numerical Methods in Fluids 18(10):983–1008

Schneck DJ (2000) An Outline of Cardiovascular Structure and Function. In: Bronzino JD (ed) The Biomedical Engineering Handbook, vol 1, 2nd edn, CRC Press, chap 1

Shankar PN (1993) The eddy structure in stokes flow in a cavity. Journal of Fluid Mechanics 250:371–383

Shen J (1991) Hopf bifurcation of the unsteady regularized driven cavity flow. Journal of Computational Physics 95(1):228–245

Sheremet MA, Pop I, Ishak A (2017) Time-dependent natural convection of micropolar fluid in a wavy triangular cavity. International Journal of Heat and Mass Transfer 105:610–622

Silber G, Janoske U, Alizadeh M, Benderoth G (2007) An application of a gradient theory with dissipative boundary conditions to fully developed turbulent flows. Journal of Fluids Engineering 129(5):643–651

Singh K (1982) Couette flow of microthermopolar fluids between two parallel plates. Acta Mechanica 43(1):1–13

Taylor C, Hood P (1973) A numerical solution of the navier-stokes equations using the finite element technique. Computers & Fluids 1(1):73–100

Tiwari RK, Das MK (2007) Heat transfer augmentation in a two-sided lid-driven differentially heated square cavity utilizing nanofluids. International Journal of Heat and Mass Transfer 50(9):2002–2018

Türk Ö, Tezer-Sezgin M (2017) FEM solution to natural convection flow of a micropolar nanofluid in the presence of a magnetic field. Meccanica 52(4):889–901

Vilchevskaya EN, Müller WH (2018) Some remarks on recent developments in micropolar continuum theory. Journal of Physics: Conference Series 991(1):012,079

Zhilin PA (2006) A micro-polar theory for binary media with application to flow of fiber suspensions. In: Indeitsev DA, Ivanova EA, Krivtsov A (eds) Advanced Problems in Mechanics, vol 2, Russian Academy of Sciences, Insitute for Problems in Mechanical Engineering